

## First Detection of Radio Linear Polarization in a Gamma Ray Burst Afterglow

YUJI URATA,<sup>1</sup> KENJI TOMA,<sup>2,3</sup> KUIYUN HUANG,<sup>4</sup> KEIICHI ASADA,<sup>5</sup> HIROSHI NAGAI,<sup>6,7</sup> SATOKO TAKAHASHI,<sup>8,9,7</sup>  
GLEN PETITPAS,<sup>10</sup> MAKOTO TASHIRO,<sup>11</sup> AND KAZUTAKA YAMAOKA<sup>12,13</sup>

<sup>1</sup>*Institute of Astronomy, National Central University, Chung-Li 32054, Taiwan*

<sup>2</sup>*Frontier Research Institute for Interdisciplinary Sciences, Tohoku University, Sendai 980-8578, Japan*

<sup>3</sup>*Astronomical Institute, Tohoku University, Sendai, 980- 8578, Japan*

<sup>4</sup>*Center for General Education, Chung Yuan Christian University, Taoyuan 32023, Taiwan*

<sup>5</sup>*Academia Sinica Institute of Astronomy and Astrophysics, Taipei 106, Taiwan*

<sup>6</sup>*National Astronomical Observatory of Japan, 2-21-1 Osawa, Mitaka Tokyo 181-8588, Japan*

<sup>7</sup>*Department of Astronomical Science, School of Physical Sciences, SOKENDAI (The Graduate University for Advanced Studies), Mitaka, Tokyo 181-8588, Japan*

<sup>8</sup>*Joint ALMA Observatory, Alonso de Cordova 3108, Vitacura, Santiago, Chile*

<sup>9</sup>*NAOJ Chile Observatory, Alonso de Cordova 3788, Oficina 61B, Vitacura, Santiago, Chile*

<sup>10</sup>*Harvard-Smithsonian Center for Astrophysics, 60 Garden Street, Cambridge, Massachusetts 02138, USA*

<sup>11</sup>*Department of Physics, Saitama University, Shimo-Okubo, Saitama, 338-8570, Japan*

<sup>12</sup>*Institute for Space-Earth Environmental Research (ISEE), Nagoya University, Furo-cho, Chikusa-ku, Nagoya, Aichi 464- 8601, Japan*

<sup>13</sup>*Division of Particle and Astrophysical Science, Graduate School of Science, Nagoya University, Furo-cho, Chikusa-ku, Nagoya, Aichi 464-8601, Japan*

### ABSTRACT

We report the first detection of radio polarization of a GRB afterglow with the first intensive combined use of telescopes in the millimeter and submillimeter ranges for GRB171205A. The linear polarization degree in the millimeter band at the sub-percent level ( $0.27 \pm 0.04\%$ ) is lower than those observed in late-time optical afterglows (weighted average of  $\sim 1\%$ ). The Faraday depolarization by non-accelerated, cool electrons in the shocked region is one of possible mechanisms for the low value. In this scenario, larger total energy by a factor of  $\sim 10$  than ordinary estimate without considering non-accelerated electrons is required. The polarization position angle varies by at least 20 degrees across the millimeter band, which is not inconsistent with this scenario. This result indicates that polarimetry in the millimeter and submillimeter ranges is a unique tool for investigating GRB energetics, and coincident observations with multiple frequencies or bands would provide more accurate measurements of the non-accelerated electron fraction.

*Keywords:* acceleration of particles, polarization, (stars:) gamma-ray burst: individual (GRB171205A)

### 1. INTRODUCTION

Gamma-ray Bursts (GRBs) are highly energetic explosions in the universe, and are currently being exploited as probes of first-generation stars and gravitational wave transients. In fact, the distant events at the re-ionization epoch (Tanvir et al. 2009; Cucchiara et al. 2011; Totani et al. 2014) and the short GRB coincident with a gravitational wave transient have already been observed (Abbott et al. 2017), respectively. The

energetics of GRBs are fundamental physical parameters that can not only reveal their progenitor systems but also probe both the early and current states of the universe (e.g., Murase et al. 2006; Toma et al. 2016; Kawaguchi et al. 2018). Although substantial observational efforts have been made since the afterglow discovery (Costa et al. 1997), the total energies have been estimated so far without considering non-accelerated, cool electrons at the relativistic collisionless shocks that do not emit observable radiation (Eichler & Waxman 2005), while the existence of such cool electrons is well studied for supernova remnants and solar winds (e.g. van Adelsberg et al. 2008; Vink et al. 2015). In

GRB afterglows, the presence of non-accelerated electrons would induce Faraday effects on the emitted radiation. Observationally, this manifests as a suppression of the radio polarization but keeps the optical polarization as emitted (Toma et al. 2008)<sup>1</sup>. Here, we report the first detection of radio polarization of a GRB afterglow through observing low-luminosity GRB 171205A, and discuss implications for the Faraday depolarization model.

GRB 171205A was detected on 5 December 2017, 07:20:43 UT (D’Elia et al. 2017) and its X-ray and optical afterglows (D’Elia et al. 2018) are identified by the Neil Gehrels Swift Observatory. Izzo et al. (2017) made spectroscopic observations with the Very Large Telescope (VLT) in Chile approximately 1.5 h after the GRB by identifying the optical afterglow and, based on the absorption and emission lines, announced a redshift of  $z = 0.0368$ . At this redshift, the isotropic  $\gamma$ -ray energy release  $E_{\gamma, \text{iso}}$  of  $2.4 \times 10^{49}$  erg (in the 20–1500 keV range with the cosmological parameters  $H_0 = 70 \text{ km s}^{-1} \text{ Mpc}^{-1}$ ,  $\Omega_m = 0.3$ , and  $\Omega_\Lambda = 0.7$ ) indicates that GRB171205A is categorized as a low-luminosity GRB. Intensive optical photometric and spectroscopic observations using the 10.4-m Gran Telescopio CANARIAS (GTC) revealed the association of a broad-line type Ic supernova that resembled SN1998bw (de Ugarte Postigo et al. 2017). The bright millimeter afterglow was also detected by the Northern Extended Millimeter Array (NOEMA) in the 90 GHz and 150 GHz bands 20.2 h after the burst (de Ugarte Postigo et al. 2017).

## 2. OBSERVATIONS AND ANALYSIS

### 2.1. SMA

Intensive total flux monitoring was made using the Submillimeter Array (SMA) at 230 GHz starting 6 December 2017 with a total of six epochs. On the nights of 8 and 13 December 2017, the afterglow was observed by the dual-band mode at 230 and 345 GHz. The data were flagged and calibrated with the MIR data-reduction package using standard procedures and were then imaged using Miriad software (Sault et al. 1995). Except for the observation at 345 GHz on 13 December 2017 (due to marginal weather conditions in the band), the afterglow was clearly detected at a confidence level of more than  $10\sigma$ . Flux measurements were performed using Common Astronomy Software Applications (CASA, version 5.1.1; McMullin et al. 2007). We measured a

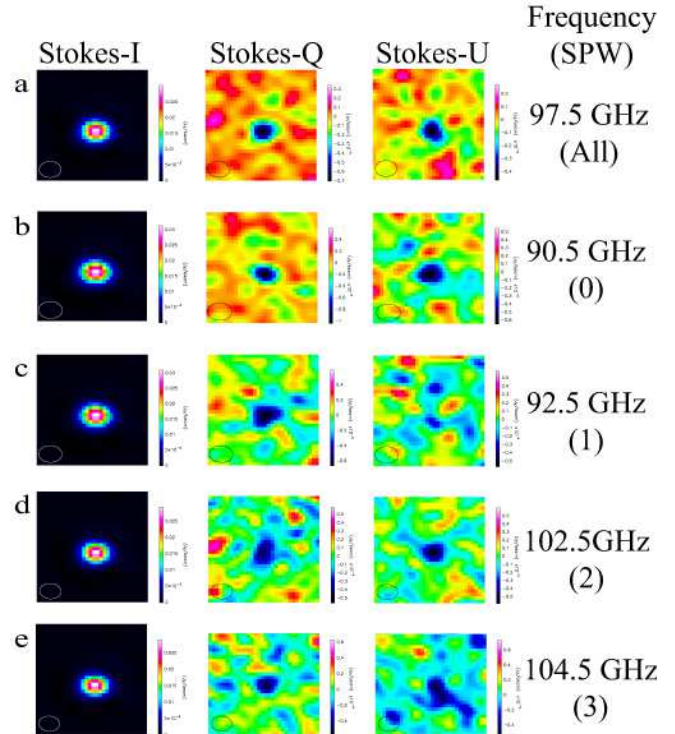


**Figure 1.** The Stokes  $I$ ,  $Q$ , and  $U$  maps ( $5'' \times 3''$ ) of the afterglow of GRB 171205A taken on 10 December 2018 (5.187 days after the burst). The ALMA beam size is shown with the open cyan circles. The map created using the entire ALMA Band 3 dataset with a representative frequency of 97.5 GHz (a), and four individual spectral windows (SPW) with a representative frequency of 90.5 GHz (b), 92.5 GHz (c), 102.5 GHz (d), and 104.5 GHz (e). The units of color bars are mJy for Stokes  $I$  and  $\mu\text{Jy}$  for Stokes  $Q$  and  $U$  maps.

bright submillimeter afterglow of  $53.7 \pm 0.9$  mJy in the 230 GHz band 1.5 days after GRB, which is the brightest afterglow ever detected in the submillimetre range. At the same epoch, the historic GRB030329 was  $49.2 \pm 1.1$  mJy in the 250 GHz band (Sheth et al. 2003), while typical submm-detected afterglows are orders of magnitude fainter (Urata et al. 2014, 2015). Thus, GRB 171205A is an ideal object for performing the first radio polarimetry.

### 2.2. ALMA

The Atacama Large Millimeter/submillimeter Array (ALMA) observed the afterglow in two different epochs using the linear polarization mode at Band 3 (representative frequency of 97.5 GHz) on 10 and 16 December 2017. The correlator processed four spectral windows (SPWs) centered at 90.5, 92.5, 102.5, and 104.5 GHz with a bandwidth of 1.75 GHz each. The bandpass and flux were calibrated using observations of J1127-1857, and J1130-1149 was used for the phase calibra-

<sup>1</sup> Spectroscopic searches of non-accelerated electrons are discussed in Ressler & Laskar (2017) and Warren et al. (2018).

tion. The polarization calibration was performed by observations of J1256-0547. The raw data were reduced at the East Asian ALMA Regional Center (EA-ARC) using CASA (version 5.1.1). We further performed iterative CLEAN deconvolution imaging with self-calibration both amplitude and phase with infinite and then 30s solution intervals). The Stokes  $I$ ,  $Q$ , and  $U$  maps were CLEANed up to 15000 of CLEAN iterations with threshold of 0.02 mJy after the final round of self-calibration (Figure 1a). The off-source rms levels in  $I$ ,  $Q$ , and  $U$  are consistent with the expectations for thermal noise alone. Since the detections with high signal to noise ratio were made on the Stokes  $Q$  and  $U$  maps generated using the entire Band 3 dataset from 10 December 2017, we generated additional Stokes maps using the individual SPWs (Figure 1b,c,d,e). The quantities that can be derived from the polarization maps are the polarized intensity ( $\sqrt{Q^2 + U^2}$ ), polarization degree ( $100\sqrt{Q^2 + U^2}/I\%$ ), and polarization position angle ( $1/2\arctan(U/Q)$ , P.A.). The *atan2* function in the python math module which returns a numeric value between  $-\pi$  and  $\pi$ , was used to calculate the polarization position angle. By applying the polarization calibration to the phase calibrator J1130-1449 and creating Stokes maps for 6, 9, and 18 epochs during the 3hr of observing period, we confirm that the stability of linear polarization degree is  $< 0.02\%$ , which is consistent with the systematic linear polarization calibration uncertainty of 0.033% for compact sources<sup>2</sup>. We also find that the stability of P.A. is  $< 0^\circ.6$ , which is slightly larger than the absolute accuracy of  $0.3^\circ$  (Nagai et al. 2016). The non-detection (both positive and negative) with  $S/N$  of 3 on the 92.5-GHz  $U$  map taken on 10 December 2017 yielded polarization position angle ranges of P.A.  $> +78^\circ$  and P.A.  $< -78^\circ$ .

The Atacama Compact Array (ACA) observations were executed on 10, 12, and 16 December 2017 at 345 GHz (Band 7) with the single continuum observing mode. Two of the ACA total flux measurements were conducted during polarimetry using ALMA. The data were flagged, calibrated and imaged with standard procedures with CASA (version 5.1.1).

### 2.3. VLA

The Very Large Array (VLA) made total flux measurements for the afterglow on 9 December 2017 at central frequencies of 6 GHz (C-band), 10 GHz (X-band), and 15 GHz (U-band), as one of the observatory-sponsored observations (Laskar et al. 2017). The phase

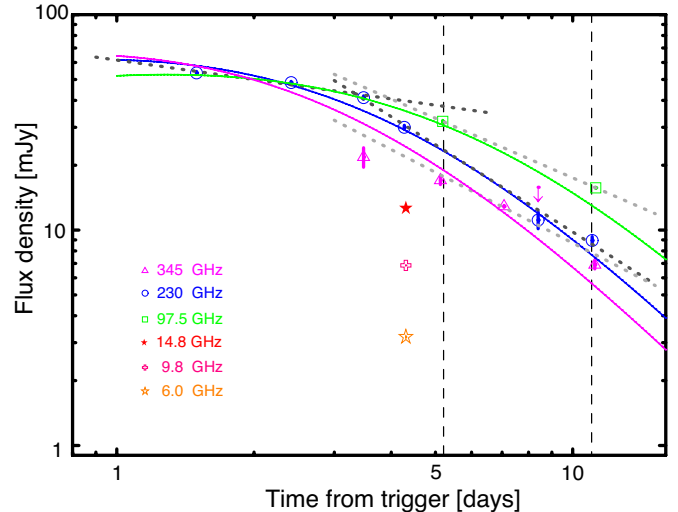


**Figure 2.** Radio afterglow light curves. Solid lines indicate the model light curves at 97.5 GHz (green), 230 GHz (blue), and 345 GHz (magenta) based on the standard forward shock model. Dark grey dotted lines show the simple power-law fittings for 230 GHz data before and 4 days after the burst. Light grey dotted lines show the simple power-law functions for 97.5 GHz with  $\alpha = -0.9$  and 345 GHz with  $\alpha = -1.2$ . Thin black dashed lines indicate the epochs of ALMA polarimetry.

and flux were calibrated using observations of J1130-1449 and 3C286. The data were calibrated using standard tools in CASA (VLA pipeline version 5.0.0). After checking the quality of the pipeline output, we performed imaging using CLEAN task without additional data flagging. The source was significantly (more than  $50\sigma$ ) detected in all three bands. To describe the spectral energy distribution, six images at the central frequencies of 5 GHz, 7 GHz, 8.5 GHz, 11 GHz, 13.5 GHz, and 16 GHz were generated with the CLEAN task. The afterglow was detected with  $>20\sigma$  significance in each image and the resulting total flux densities are summarized in Table 1.

## 3. RESULTS

### 3.1. Lightcurve and SED

The temporal evolution of the afterglow flux at 230 GHz is described by broken power-law decays ( $F_\nu \propto t^\alpha$ ) with  $\alpha = -0.30 \pm 0.07$  for  $t \lesssim 4$  days and  $\alpha = -1.34 \pm 0.06$  for  $t \gtrsim 4$  days, as show in Figure 2. The light curve at 345 GHz for  $t \gtrsim 4$  is also described by a simple power-law with  $\alpha = -1.2 \pm 0.2$ . The spectral slope ( $F_\nu \propto \nu^\beta$ ) is also described as  $\beta = 1.457 \pm 0.028$  at 4.3 days in the centimeter range (5–16 GHz; Figure 3a) and  $\beta = -0.430 \pm 0.004$  at 5.2 days in the submillimeter and millimeter range (90.5–345 GHz; Figure 3a). High-quality photometry ( $S/N \sim 72$ –89) using ALMA during

<sup>2</sup> ALMA technical handbook; <https://almascience.nrao.edu/documents-and-tools/cycle7/alma-technical-handbook/>

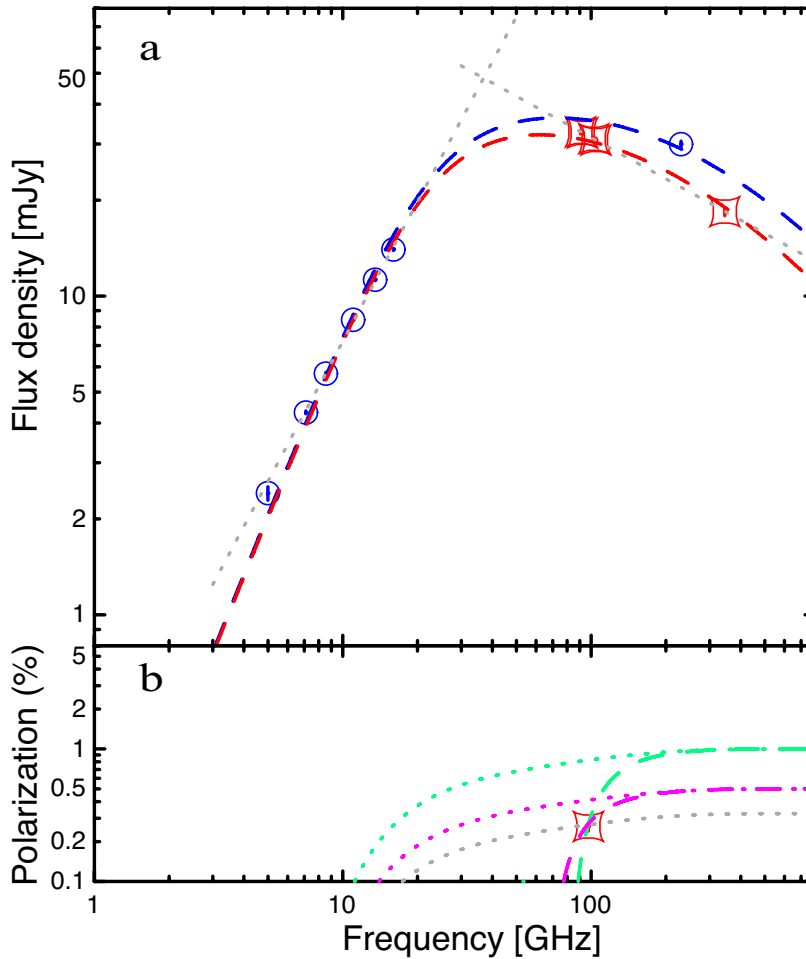


**Figure 3.** Spectral flux distributions and total linear polarization spectrum of the GRB 171205A afterglow. a, Spectral flux distribution at 4.1 days (blue circles and model dashed line) and 5.2 days (red squared points and model dashed line) after burst. The grey dotted lines indicate the simple power-law functions with index of 1.457 and -0.430. b, Total linear polarization spectrum with the ALMA measurement 5.2 days after the burst. Dashed lines indicate the Faraday depolarized spectrum by assuming  $P_0$  of 1% (green) and 0.5% (magenta). The dotted lines indicate the polarization spectrum without the Faraday depolarization effect (i.e. all electrons are energized by the relativistic shock) by assuming  $P_0$  of 1% (green), 0.5% (magenta), and 0.33% (grey).

the polarimetry, at 5.2 days, measured the spectral slope of  $\beta = -0.40 \pm 0.01$  in the 90–100 GHz (i.e. Band 3). These measurements indicate that the spectral peak was located at  $\sim 30$  GHz (below  $\sim 90$  GHz).

### 3.2. Polarization

Figure 1a shows the Stokes  $I$ ,  $Q$ , and  $U$  maps obtained using the entire ALMA Band 3 frequency range taken 5.2 days after the GRB. Detections with a confidence level of  $5\sigma$  or better on the  $Q$  and  $U$  maps yield a polarization degree of  $0.27 \pm 0.04\%$  (including systematic error). Our measured value describes the intrinsic origin because depolarization between the source and observing site is negligible for the point source (i.e. GRB afterglows) in this millimeter band (Brentjens & de Bruyn 2005). Although we could not find any detection in the

Stokes  $Q$  and  $U$  maps at 11.2 days, we measured the corresponding deep upper limit of the polarization degree ( $< 0.27\%$ ,  $3\sigma$  significance), which was consistent with that at 5.2 days within the error margin.

The apparent brightness of  $31.94 \pm 0.44$  mJy observed 5.2 days after the burst using the entire ALMA Band 3 frequency range enabled more detailed polarimetric analysis using four individual spectral windows (SPW) of Band 3 (Figure 1 b, c, d, and e). The measurements are summarized in Table 1. Other than the Stokes  $U$  map at 92.5 GHz, there were significant detections at a  $3.0\sigma$  confidence level or better. In the Stokes  $U$  map at 92.5 GHz, there was no significant flux, and the range of the P.A. was constrained. Although the polarization degrees in each SPW were consistent with the value measured using the entire Band 3 frequency, the P.A. significantly

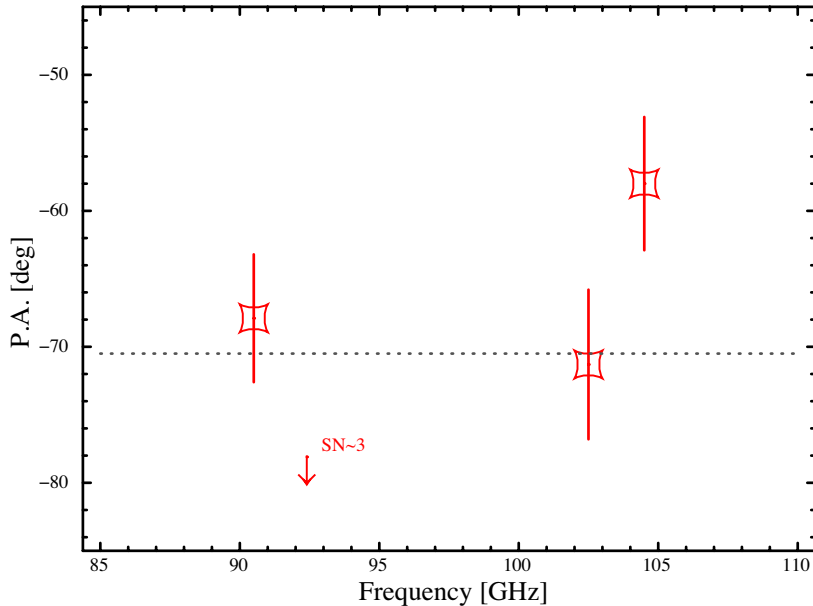


**Figure 4.** The position angle (P.A.) of the GRB171205A afterglow as a function of wavelength. Squared points indicate the observed P.A. at 90.5, 102.5, 104.5 GHz. The upper limit at 92.5 GHz with a signal-to-noise ratio of 3 is also plotted with a red arrow. The grey dotted line indicates the constant fitting function with a reduced chi-square of 4.5 (d.o.f = 3).

varied with the wavelength (Figure 4). The observed P.A. is most likely intrinsic value because the Faraday rotation effect for both the host galaxy and Milky Way Galaxy is quite small at this frequency (Sokoloff et al. 1998; Oppermann et al. 2012). The expected galactic Faraday rotation effect is up to  $\sim 0.3^\circ$ . We tried to fit the P.A. data including the upper limit (the method is described in Sawicki 2012) with constant or linear function of squared wavelength, but did not obtain a good fit (Figure 4).

## 4. DISCUSSION

### 4.1. Afterglow modeling

We find that the spectra of Figure 3a can be well fitted by the forward shock synchrotron emission model by Granot & Sari (2002) with the synchrotron self-absorption frequency  $\nu_a \sim 20$  GHz and the synchrotron frequency of minimum-energy electrons  $\nu_m \sim 200$  GHz. In such a late phase the slow cooling regime (i.e.  $\nu_m < \nu_c$ ) is likely. Then the observed shallow decay at  $t \lesssim 4$  days may correspond to the spectral segment  $\nu_a < \nu < \nu_m$ . If the spectrum in this segment is the power-law with  $\beta = 1/3$ , the decay index is  $\alpha = 3\beta/2 - 1/2 = 0$  in the wind environment case (Zhang & Mészáros 2004). However, our smoothly broken power-law spectrum ( $\beta < 1/3$  effectively, see Figure 3a) leads to a steeper decay, which cannot fit the observed 230 GHz light curve at  $t \lesssim 4$  days. Alternatively, we find that the ISM environment case can well fit it.

The flux after  $\nu_m$  crosses the observed frequency (i.e.  $\nu_m < \nu < \nu_c$ ) obeys the closure relation  $\alpha - 3\beta/2 = 0$  (Zhang & Mészáros 2004) in the ISM environment case when the edge of the collimated shock is not observed. After the edge is observed (but the shock does not expand sideways; Zhang & MacFadyen 2009), the additional geometrical flux reduction  $\Gamma^2\theta_j^2 \propto t^{-3/4}$  leads to  $\alpha - 3\beta/2 = -3/4$ , where  $\Gamma$  and  $\theta_j$  are the Lorentz factor and opening half-angle of the shock, respectively. The latter relation is consistent with the observed relation  $\alpha - 3\beta/2 \simeq -0.69 \pm 0.07$ .

Based on the above consideration, we adopt the flux formula of Granot & Sari (2002) multiplied by the geometrical flux reduction factor  $[1 + (t/t_j)]^{-3/4}$  to fit the observed data (Figure 2, 3a). Here we set the synchrotron self-absorption frequency  $\nu_a \simeq 22$  GHz, the synchrotron frequency of minimum-energy electrons  $\nu_m \simeq 200 (t/4.3 \text{ days})^{-3/2}$  GHz, the peak flux before the jet break  $F_{\nu_m}(t < t_j) \simeq 72$  mJy, the jet break time  $t_j \simeq 2$  days, and the electron energy spectral index  $p \simeq 3$ . The first three characteristic quantities are functions of four physical parameters, namely the isotropic shock energy  $E_{\text{iso}}$ , the ambient medium density  $n$ , the fraction of shock energy carried by the electrons  $\epsilon_e$ , and that carried by amplified magnetic field  $\epsilon_B$ . Thus, we have the relations  $n \simeq 600 (E_{\text{iso}}/5 \times 10^{48} \text{ erg})^3 \text{ cm}^{-3}$ ,  $\epsilon_e \simeq 0.3 (E_{\text{iso}}/5 \times 10^{48} \text{ erg})$ , and  $\epsilon_B \simeq 0.2 (E_{\text{iso}}/5 \times 10^{48} \text{ erg})^{-5}$ . The numerical values of  $n$ ,  $\epsilon_e$ , and  $\epsilon_B$  are not unrealistic (Panaitescu & Kumar 2002), and  $E_{\text{iso}}$  should not be considerably different from this value be-

cause of  $\epsilon_e < 1$  and  $\epsilon_B < 1$ . For these values we calculated X-ray light curve, which does not overwhelm the observed one. This analysis means that we found a possible physical afterglow model (while we leave a full exploration of possible models to separate work), and supports our argument that we performed the first radio afterglow polarimetry in the waveband well above  $\nu_a$  (c.f. Granot & Taylor 2005; van der Horst et al. 2014).

#### 4.2. Faraday depolarization effect

We focused on the polarization at 5.2 days, the phase when the intensity can be explained by the standard forward shock model. The precise detection of the polarization degree of  $0.27 \pm 0.04\%$  indicated that the value is the smallest one among all afterglow polarization measurements, and smaller than those in late-time optical afterglows explained by the standard forward shock model, which range from 0.5% to 10% (Greiner et al. 2003; Wiersema et al. 2014; Covino & Gotz 2016)<sup>3</sup>.

There was no polarimetric data at the higher frequency ranges for the present event (except the supernova component in the optical band). Note that there are 84 polarimetric measurements for optical afterglows (i.e. excluding measurements for early-time reverse shock components that show high values) among 13 GRBs (Covino & Gotz 2016). The weighted average and average of the measurements are 1.0% and 1.6%, respectively. Among these, 58 measurements were made during the phases in which the intensities are describable by the standard forward shock model. For these selected events, the weighted average and average of the linear polarizations are 1.2% and 1.7%, respectively.

By assuming a polarization degree at higher frequency ranges (e.g. optical) for the present event as  $P_0 = 1\%$ , we calculate the polarization spectrum based on the afterglow model described above (c.f. Matsumiya & Ioka 2003; Sagiv et al. 2004; Jones & O’Dell 1977; Huang & Shcherbakov 2011), and plot it by the green dotted line in Figure 3b. It varies by a factor of  $0.5(p + 7/3)/(p + 1) \simeq 2/3$  at  $\nu = \nu_m$  and decays at  $\nu \lesssim \nu_a$ . Our measured value is substantially lower than this model line.

If only part of the swept-up electrons is accelerated, the non-accelerated electrons with thermal Lorentz factor  $\tilde{\gamma}_m = \eta\Gamma$  cause Faraday depolarization at  $\nu > \nu_a$  (Toma et al. 2008), where  $\eta$  is a factor of the order of unity in the case that the non-accelerated electrons are just isotropized at the shock front (Eichler & Waxman

2005). Such a model in which the fraction of accelerated electrons is  $f < 1$  can explain the intensity in the same way as in the standard model with the parameters  $E'_{\text{iso}} = E_{\text{iso}}/f$ ,  $n' = n/f$ ,  $\epsilon'_e = \epsilon_e f$ , and  $\epsilon'_B = \epsilon_B f$  (Eichler & Waxman 2005). Thus, a very small value of  $f$  would lead to a crisis of the total energy requirement. In this scenario, the polarization degree is given by  $P_0 \sin(\tilde{\tau}_V/2)/(\tilde{\tau}_V/2)$  where  $\tilde{\tau}_V = (\nu/\tilde{\nu}_V)^{-2}$  and  $\tilde{\nu}_V \sim 200 [(1-f)/10f]^{1/2} \eta^{-1} \sqrt{\ln \tilde{\gamma}_m} N^{-1/12} (E_{\text{iso}}/10^{52} \text{ erg})^{3/16} n^{9/16} (\epsilon_B/0.01)^{1/4} (t/1 \text{ day})^{-1/16}$  GHz. Here the magnetic field in the shocked region has been assumed to be tangled on hydrodynamic scales, following Toma et al. (2008) and Uehara et al. (2012), and then the plasma can be considered to consist of a number of random cells, in each of which magnetic field is ordered (Jones & O’Dell 1977; Gruzinov & Waxman 1999).  $N$  denotes the number of random cells in the three-dimensional visible region. In this case  $P_0 = (p + 1)/[(p + 7/3)\sqrt{N}]$  for  $\nu > \nu_m$  while  $P_0 = 0.5/\sqrt{N}$  for  $\nu_a < \nu < \nu_m$ . With  $P_0 = 1\%$  for  $\nu > \nu_m$ ,  $\tilde{\nu}_V \simeq 210$  GHz explains our measurement (see the green dashed line in Figure 3b), which corresponds to  $1/f \sim 12 (E_{\text{iso}}/2 \times 10^{50} \text{ erg})^{-5/4} \eta^2 (\ln \tilde{\gamma}_m)^{-1}$ . For the case of  $P_0 = 0.5\%$  (Figure 3b),  $1/f \sim 10$  is still required. For the case of  $P_0 = 10\%$ ,  $1/f \sim 60$  is required. We should also note that the case of  $P_0 \simeq 0.33\%$  is not ruled out (see Figure 3b), where the Faraday depolarization effect with  $f < 1$  is not required.

The P.A. becomes a very complicated function of wavelength and the functional form is determined randomly for such a tangled magnetic field that we assume (Sokoloff et al. 1998). Therefore, the observed variation of the P.A. is not inconsistent with this scenario.

In summary, with the first intensive combined use of telescopes in the millimeter and submillimeter ranges for the GRB171205A afterglow, our observations provided the first linear polarimetry in the millimeter band. The measured polarization degree is substantially lower than the typical optical one. Although the (semi-) simultaneous measurements in multiple wavelengths are required, this measurement suggests the Faraday depolarization effect and larger total energy by a factor of  $\sim 10$  than ordinary estimate without considering non-accelerated electrons. The observed P.A. variation along with wavelength is not inconsistent with this scenario. Multi-frequency polarimetry in the submillimeter/millimeter range and/or with simultaneous optical polarimetry would provide more accurate non-accelerated electron fraction. Hence, this observation consolidates the new methodology for revealing the fundamental properties of GRBs.

<sup>3</sup> Although the minimum value of 0.31% was measured with the GRB030329 optical afterglow, the measurement was performed during the multiple bump light curve phase with strong polarization variabilities (i.e. extra physical explanations to the standard afterglow model are required).

**Table 1.** Polarization and Photometric Observing Log

Polarimetry Epoch1: 2017-12-10 10:23-13:17, T=5.187 days						
SPW	Frequency [GHz]	Pol. [%]	P.A. [deg]	I flux [mJy]	Q flux [mJy]	U flux [mJy]
0,1,2,3	97.5	0.27±0.04	-71.3±3.3	31.944±0.440	-0.069±0.009	-0.053±0.011
0	90.5	0.30±0.06	-67.9±4.7	32.719±0.413	-0.070±0.010	-0.069±0.020
1	92.4	<0.32	< -78.1 or >78.1	32.514±0.365	-0.094±0.026	0.014(rms)
2	102.5	0.35±0.08	-71.3±5.5	31.172±0.399	-0.086±0.025	-0.066±0.018
3	104.5	0.31±0.06	-58.0±4.9	30.898±0.412	-0.043±0.012	-0.087±0.029
Polarimetry Epoch2: 2017-12-16 11:14-14:33, T=11.231 days						
SPW	Frequency [GHz]	Pol. [%]	P.A. [deg]	I flux [mJy]	Q flux [mJy]	U flux [mJy]
All	97.5	<0.27	—	15.705±0.090	0.010 (rms)	0.010 (rms)
0	90.5	<0.52	—	16.171±0.106	0.020 (rms)	0.020 (rms)
1	92.4	<0.52	—	16.054±0.110	0.019 (rms)	0.019 (rms)
2	102.5	<0.52	—	15.370±0.113	0.019 (rms)	0.019 (rms)
3	104.5	<0.54	—	15.206±0.111	0.019 (rms)	0.019 (rms)
Total Flux Observation Log						
Instrument	Epoch [days]	Frequency [GHz]	Flux [mJy]			
VLA	4.306	5.0	2.41±0.12			
VLA	4.306	7.1	4.32±0.05			
VLA	4.306	8.5	5.71±0.05			
VLA	4.306	11.0	8.42±0.06			
VLA	4.306	13.5	11.26±0.09			
VLA	4.306	16.0	14.01±0.11			
SMA	1.496	230	53.6±0.9			
SMA	2.412	230	48.4±0.6			
SMA	3.478	230	41.2±0.8			
SMA	4.272	230	30.0±0.7			
SMA	8.398	230	11.1±1.0			
SMA	11.033	230	8.9±0.4			
SMA	3.478	345	21.9±2.3			
ACA	5.126	345	17.0±0.8			
ACA	7.069	345	12.9±0.1			
SMA	8.398	345	>15.8			
ACA	11.180	345	6.9±0.3			

We thank the anonymous referee for his/her careful review of our manuscript. This paper makes use of the following ALMA data: ADS/JAO.ALMA#2017.1.00801.T. ALMA is a partnership of ESO (representing its member states), NSF (USA), and NINS (Japan), together with NRC (Canada), MOST and ASIAA (Taiwan), and KASI (Republic of Korea), in cooperation with the Republic of Chile. The Joint ALMA Observatory is operated by ESO, AUI/NRAO, and NAOJ. This work is supported by the Ministry of Science and Technology of Taiwan grants MOST 105-2112-M-008-013-MY3 (Y.U.) and 106-2119-M-001-027 (K.A.). This work is also sup-

ported by JSPS Grants-in-Aid for Scientific Research No. 18H01245 (K.T.). We thank EA-ARC, especially Pei-Ying Hsieh for support in the ALMA observations. We also thank P. T. P. Ho and Y. Ohira for helpful comments. Y.U, K. Y. H, and K. A. also thank Ministry of Education Republic of China.

*Facilities:* ALMA, SMA, VLA

*Software:* CASA (McMullin et al. 2007),

## REFERENCES

- Abbott, B. P., Abbott, R., Abbott, T. D., et al. 2017, ApJL, 848, L13
- Brentjens, M. A., & de Bruyn, A. G. 2005, A&A, 441, 1217

- Costa, E., Frontera, F., Heise, J., et al. 1997, *Nature*, 387, 783
- Covino, S., & Gotz, D. 2016, *Astronomical and Astrophysical Transactions*, 29, 205
- Cucchiara, A., Levan, A. J., Fox, D. B., et al. 2011, *ApJ*, 736, 7
- D’Elia, V., D’Ai, A., Lien, A. Y., & Sbarufatti, B. 2017, *GRB Coordinates Network, Circular Service*, No. 22177, #1 (2017), 22177, 1
- D’Elia, V., Campana, S., D’Ai, A., et al. 2018, *A&A*, 619, A66
- de Ugarte Postigo, A., Izzo, L., Kann, D. A., et al. 2017, *GRB Coordinates Network, Circular Service*, No. 22204, #1 (2017), 22204, 1
- de Ugarte Postigo, A., Schulze, S., Bremer, M., et al. 2017, *GRB Coordinates Network, Circular Service*, No. 22187, #1 (2017), 22187, 1
- Eichler, D., & Waxman, E. 2005, *ApJ*, 627, 861
- Granot, J., & Sari, R. 2002, *ApJ*, 568, 820
- Granot, J., & Taylor, G. B. 2005, *ApJ*, 625, 263
- Greiner, J., Klose, S., Reinsch, K., et al. 2003, *Nature*, 426, 157
- Gruzinov, A., & Waxman, E. 1999, *ApJ*, 511, 852
- Huang, L. & Shcherbakov, R. V. 2011, *MNRAS*, 416, 2574
- Izzo, L., Selsing, J., Japelj, J., et al. 2017, *GRB Coordinates Network, Circular Service*, No. 22180, #1 (2017), 22180, 1
- Jones, T. W., & O’Dell, S. L. 1977, *ApJ*, 214, 522
- Kawaguchi, K., Shibata, M., & Tanaka, M. 2018, *ApJL*, 865, L21
- Laskar, T., Coppejans, D. L., Margutti, R., & Alexander, K. D. 2017, *GRB Coordinates Network, Circular Service*, No. 22216, #1 (2017), 22216, 1
- Matsumiya, M., & Ioka, K. 2003, *ApJ*, 595, L25
- McMullin, J. P., Waters, B., Schiebel, D., Young, W., & Golap, K. 2007, *Astronomical Data Analysis Software and Systems XVI*, 376, 127
- Murase, K., Ioka, K., Nagataki, S., et al. 2006, *ApJL*, 651, L5
- Nagai, H., Nakanishi, K., Paladino, R., et al. 2016, *ApJ*, 824, 132
- Oppermann, N., Junklewitz, H., Robbers, G., et al. 2012, *A&A*, 542, A93
- Panaitescu, A., & Kumar, P. 2002, *ApJ*, 571, 779
- Ressler, S. M., & Laskar, T. 2017, *ApJ*, 845, 150
- Sagiv, A., Waxman, E., & Loeb, A. 2004, *ApJ*, 615, 366
- Sault, R. J., Teuben, P. J., & Wright, M. C. H. 1995, *Astronomical Data Analysis Software and Systems IV*, 77, 433
- Sawicki, M. 2012, *PASP*, 124, 1208
- Sheth, K., Frail, D. A., White, S., et al. 2003, *ApJL*, 595, L33
- Sokoloff, D. D., Bykov, A. A., Shukurov, A., et al. 1998, *MNRAS*, 299, 189
- Tanvir, N. R., Fox, D. B., Levan, A. J., et al. 2009, *Nature*, 461, 1254
- Toma, K., Ioka, K., & Nakamura, T. 2008, *ApJL*, 673, L123
- Toma, K., Yoon, S.-C., & Bromm, V. 2016, *SSRv*, 202, 159
- Totani, T., Aoki, K., Hattori, T., et al. 2014, *PASJ*, 66, 63
- Uehara, T. et al. 2012, *ApJ*, 752, L6
- Urata, Y., Huang, K., Takahashi, S., et al. 2014, *ApJ*, 789, 146
- Urata, Y., Huang, K., Asada, K., et al. 2015, *Advances in Astronomy*, 2015, 165030
- van Adelsberg, M., Heng, K., McCray, R., & Raymond, J. C. 2008, *ApJ*, 689, 1089
- van der Horst, A. J., Paragi, Z., de Bruyn, A. G., et al. 2014, *MNRAS*, 444, 3151
- Vink, J., Broersen, S., Bykov, A., & Gabici, S. 2015, *A&A*, 579, A13
- Warren, D. C., Barkov, M. V., Ito, H., Nagataki, S., & Laskar, T. 2018, *MNRAS*, 480, 4060
- Wiersema, K., Covino, S., Toma, K., et al. 2014, *Nature*, 509, 201
- Zhang, B., & Mészáros, P. 2004, *International Journal of Modern Physics A*, 19, 2385
- Zhang, W., & MacFadyen, A. 2009, *ApJ*, 698, 1261